

# Critical exponents of a three dimensional $O(4)$ spin model

K. Kanaya and S. Kaya

*Institute of Physics, University of Tsukuba, Ibaraki 305, Japan*

## Abstract

By Monte Carlo simulation we study the critical exponents governing the transition of the three-dimensional classical  $O(4)$  Heisenberg model, which is considered to be in the same universality class as the finite-temperature QCD with massless two flavors. We use the single cluster algorithm and the histogram reweighting technique to obtain observables at the critical temperature. After estimating an accurate value of the inverse critical temperature  $K_c = 0.9360(1)$ , we make non-perturbative estimates for various critical exponents by finite-size scaling analysis. They are in excellent agreement with those obtained with the  $4-\epsilon$  expansion method with errors reduced to about halves of them.

# 1 Introduction

Finite temperature chiral phase transition of QCD is very important in the study of phase transitions in the early Universe and in the investigation of heavy ion collisions at high energy. At present, this transition is studied mainly using the Monte Carlo method on the lattice. Pisarski and Wilczek [1, 2] suggested that QCD with massless two flavors, which is considered to be an approximation of the real world, belongs to the same universality class as three-dimensional four-component Heisenberg models, if the finite temperature chiral transition of  $N_f = 2$  QCD is second order. Then, the chiral transition of  $N_f = 2$  QCD has the same critical exponents as the 3d O(4) Heisenberg model.

Simulations of lattice QCD for  $N_f = 2$  suggest that the chiral transition is a second order transition for staggered fermions [3] and for Wilson fermions [4]. The study towards a precise measurement of the critical exponents of  $N_f = 2$  QCD has just begun [5]. In the verification that the O(4) Heisenberg model belongs to the same universality class, there is a problem that both Wilson fermions and staggered fermions on the lattice do not have the full chiral symmetry — which is expected to restore only in the continuum limit. Conversely, however, we could consider that, assuming the universality, the chiral symmetry is restored on the lattice sufficiently when the exponents agree with those of the 3d O(4) Heisenberg model.

Therefore an accurate calculation of the critical exponents of the 3d O(4) Heisenberg model is quite important. For this model the best estimation of critical exponents has been made with the  $4 - \epsilon$  expansion method up to seven loops [6].

In this work we simulate the 3d O(4) Heisenberg model by the Monte Carlo method and make a non-perturbative estimation of several critical exponents. We use the single cluster Monte Carlo update algorithm which recently has been used for the simulation of spin systems: Wolff formulated this algorithm by modifying the multiple-cluster algorithm by Swendsen and Wang[7] and applied it to continuous spin models[8, 9]. Recent applications of the multiple and single cluster algorithms to two and three dimensional spin models have demonstrated their advantage in the computation time to the usual local update algorithms. Among global algorithms, the single-cluster algorithm is shown to be superior to the multiple-cluster algorithm

for three-dimensional spin models[10, 11]. Therefore, we apply the single-cluster algorithm in this study.

In section 2 the model and the method of simulation are described. In section 3 we estimate the transition point from the crossing point of the Binder cumulant and compute the critical exponents at the transition point making use of the histogram reweighting technique. We also check the consistency of the results by independent measurements of the critical temperature and several exponents. We then compare our exponents with those of the  $4 - \epsilon$  expansion method. Our conclusion is given in section 4.

## 2 The model and the method

The partition function  $Z$  and the energy  $E$  of the 3d O(4) Heisenberg model are defined by

$$\begin{aligned} Z &= \prod_{\mathbf{x}} \int [d\vec{s}] e^{(-KE)}, \\ E &= \sum_{\mathbf{x}, \hat{i}} \{1 - \vec{s}(\mathbf{x}) \cdot \vec{s}(\mathbf{x} + \hat{i})\}, \end{aligned} \quad (1)$$

where  $K$  is the inverse temperature and  $\vec{s}(\mathbf{x})$  is a four-dimensional unit spin at the lattice site  $\mathbf{x}$ .  $\hat{i}$ 's are the unit steps in three coordinate directions. We use three-dimensional simple cubic lattices with the volume  $V = L^3$  with  $L = 8, 10, 12, 14, 16, 24,$  and  $32$ , and employed periodic boundary conditions.

We chose two simulation points for each  $L$  except for  $L = 10$ : One is  $K = 0.935$  which is a rough estimate for the transition point by our preparatory simulation. Another simulation point is chosen for each  $L$  at the maximum point of the susceptibility estimated by a preparatory simulation. Our simulation parameters are compiled in Table 1. We use the data at  $K = 0.935$  for the calculation of the transition point as well as the analyses of finite-size scaling with the histogram reweighting technique and use the data at the maximum of the susceptibility for a check of the consistency of our results.

The magnetization and the energy are measured every 10 sweeps and stored on the disk. We define one sweep by one cluster update by the single-cluster algorithm

explained in the following section. Several million sweeps are performed for each simulation point. From the autocorrelation time we measured (see the following section) this corresponds to about one hundred thousand independent data for each point, as compiled in Table 1. We estimate errors by the jackknife procedure. We study the bin-size dependence of errors and choose a sufficiently large bin-size such that errors become stable. The resulting bin-sizes are consistent with the values of auto-correlation time estimated independently. All the jobs takes 23 hours with HITAC S820/80.

We use the histogram reweighting method[12] to calculate the observables in a region of  $K$  around the simulated point  $K_{simu}$ . The region of  $K$  in which the histogram reweighting method is applicable can be determined by the magnitude of the shift of energy value: If the peak position of a reweighted energy distribution,  $E_{peak}(K)$ , locates away from the peak position of the original distribution,  $E_{peak}(K_{simu})$ , then the statistical errors for averages computed with the reweighted distribution become large correspondingly. Limited statistics near the tails of measured histograms also leads to a danger of large under-estimation of the errors there. We study the effect of reweighting and observe that, with our statistics, many errors for the observables we study become rapidly large and the histogram becomes rapidly notched when  $K$  gets outside the region where the height of the original energy histogram at  $E_{peak}(K)$  is larger than one third of the peak height. Although several computed errors, such as the error for the Binder cumulant discussed below, sometimes remain small even outside this range, we find that the result is not consistent with the result of a direct simulation there. We therefore limit ourselves to apply the histogram reweighting method only up to the point where the height of the original energy histogram at  $E_{peak}(K)$  decreases to a third of the peak height. Similar criterion is used also in Ref. [13].

## 2.1 Algorithm

We use the single-cluster algorithm formulated by Wolff[8]. This is a global update algorithm whose advantage is that the autocorrelation time and the dynamical exponent are both much smaller than those of the local update algorithm as discussed

below.

The autocorrelation function  $A(k)$  is defined by

$$\begin{aligned} A(k) &= \frac{\rho(k)}{\rho(0)}, \\ \rho(k) &= \langle O_i O_{i+k} \rangle - \langle O_i \rangle^2, \end{aligned} \quad (2)$$

with  $O_i$  being the  $i$ -th measurement of an observable  $O$ . The autocorrelation time  $\tau$  which is given by integrating the autocorrelation function

$$\tau = \sum_{k=1}^{\infty} A(k) \quad (3)$$

diverges in the critical region as  $\tau \propto \xi^z$ , where  $\xi$  is the correlation length. The exponent  $z$  is called as dynamical exponent. On finite lattices in the critical region,  $\xi$  is replaced by the lattice length  $L$ :

$$\tau \propto L^z. \quad (4)$$

This lattice size dependence of  $\tau$  is the origin of the ‘‘critical slowing down’’ which makes difficult to get a high effective statistics in the critical region on large lattices. We should use an algorithm with a small dynamical exponent. It is known that the local update algorithms such as the Metropolis algorithm have  $z \sim 2$  independent of the model and the details of the update algorithm. For example,  $z = 1.94(6)$  is obtained for the 3d  $O(3)$  Heisenberg model with Metropolis algorithm[14]. Use of a global update algorithm is required to get a smaller  $z$ . It is reported in Refs.[10, 13, 15] that  $z$  with the single-cluster algorithm for the 3d Ising model is about 0.2 and that for the 3d  $O(3)$  Heisenberg model is about 0. As presented in the next section, our result of  $z$  for the 3d  $O(4)$  Heisenberg model is also consistent with 0.

The single-cluster update for the  $O(n)$  Heisenberg model is as follows [8, 16]:

- (1) A unit vector in the  $O(n)$  space,  $\vec{r}$ , is chosen with a random direction.
- (2) A starting site of a cluster,  $\mathbf{x}_0$ , is chosen at random and is included in the cluster.
- (3) For a link on the surface of the cluster,  $\partial_C = \{(\mathbf{x}, \mathbf{y}) | \mathbf{x} \in C, \mathbf{y} \notin C\}$ ,  $\mathbf{y}$  is included in the cluster with the probability

$$P(\vec{s}_{\mathbf{x}}, \vec{s}_{\mathbf{y}}) = 1 - \exp[\min\{0, -2K(\vec{r} \cdot \vec{s}_{\mathbf{x}})(\vec{r} \cdot \vec{s}_{\mathbf{y}})\}]. \quad (5)$$

- (4) The process (3) is repeated until the growth of the cluster stops.
- (5) All spins in the cluster is flipped with regards to the surface perpendicular to  $\vec{r}$ :

$$\vec{s}'_{\mathbf{x}} = R(\vec{r})\vec{s}_{\mathbf{x}} = \vec{s}_{\mathbf{x}} - 2(\vec{s}_{\mathbf{x}} \cdot \vec{r})\vec{r}. \quad (6)$$

In order to test the efficiency of the algorithm and to test our program code for the single-cluster update, we simulate the 3d Ising and the 3d O(3) Heisenberg model. Our results are completely consistent with Refs.[10, 13], including the results for susceptibility, dynamical exponent, and critical exponents.

## 3 Results

### 3.1 Autocorrelation time and energy distribution

Our results for the autocorrelation time are compiled in Table 1. The autocorrelation time  $\tau_m$  in terms of Metropolis unit stays almost constant or rather decreases with the increase of the lattice size. This implies that the dynamical exponent is 0 or slightly smaller than 0. Similar result is obtained also for the O(3) Heisenberg model[13].

The measured energy distribution shown in Fig. 1 is a Gaussian type with single peak. The continuous shift of the distribution with the temperature over the expected critical region is consistent with a second order phase transition in accord with the results of the  $4 - \epsilon$  expansion method. Final confirmation of the order of the transition is done with the values of the critical exponents discussed below.

### 3.2 Critical temperature

Accurate calculation of critical exponents requires a precise determination of the inverse critical temperature  $K_c$ . An efficient method to determine  $K_c$  for a second order transition is to measure the Binder cumulant [17] for various system size and to locate the cross point in the space of  $K$ . On sufficiently large lattices where subleading corrections from the finite lattice size  $L$  are ignored, the Binder cumulant

$U_L(K)$  defined by

$$U_L(K) = 1 - \frac{1}{3} \frac{\langle m^4 \rangle}{\langle m^2 \rangle^2}$$

$$\vec{m} = \frac{1}{V} \sum_{\mathbf{x}} \vec{s}(\mathbf{x}), \quad (7)$$

becomes independent of  $L$  at the transition point  $K_c$  [17]:

$$\frac{U_{L'}(K_c)}{U_L(K_c)} = 1, \quad (8)$$

and the slope of  $U_L(K)$  in  $K$  at  $K_c$  increases as  $L$  becomes large. In Fig.2 are shown our results of the Binder cumulant near the crossing point. The values for  $U_L(K)$  are obtained with the histogram method using the data at  $K=0.935$ .

The deviation from the relation (8) observed in Fig.2 can be explained by the finite-size confluent corrections. The leading  $L'/L$ -dependence in the deviation of the crossing point  $K^*$  from the critical point  $K_c$  is estimated by Binder[17] as

$$\frac{1}{K_c} - \frac{1}{K^*} \propto \frac{1}{\ln b} \quad (9)$$

where  $b = L'/L$ .

We plot  $(1/\ln b, 1/K^*)$  for  $L = 8, 10, 12,$  and  $14$  in Fig. 3. The errors for  $1/K^*$  are computed from the jackknife errors for  $U_L(K)$ . The solid lines in Fig. 3 represent the results of a linear least-square fit for each  $L$ . We find that the correction with  $1/\ln b$  is smaller than that of 3d O(3) Heisenberg model [13]. The extrapolation of  $1/K^*$  to the point  $1/\ln b = 0$  for each  $L$  gives the values for  $1/K_c(L)$ :  $1/K_c(8) = 1.06841(21)$ ,  $1/K_c(10) = 1.06832(26)$ ,  $1/K_c(12) = 1.06833(26)$ ,  $1/K_c(14) = 1.06826(34)$ . All of them are consistent with each other. The mean value of these results is  $1/K_c = 1.06835(13)$ . A similar fit for all  $L$  with a common parameter  $1/K_c$  gives the value  $1/K_c = 1.06836(14)$  which completely agrees with the mean value. We quote hereafter

$$\frac{1}{K_c} = 1.06835(13), \quad (10)$$

$$K_c = 0.9360(1). \quad (11)$$

### 3.3 The critical exponent $\nu$

The slope for  $\left. \frac{dU_L}{dK} \right|_{K=K_c}$  is known to scale with a critical exponent  $\nu$  as [17]

$$\left. \frac{dU_L}{dK} \right|_{K=K_c} \sim L^{1/\nu}. \quad (12)$$

Using the relation

$$\frac{dU_L}{dK} = (1 - U_L) \left\{ \langle E \rangle - 2 \frac{\langle m^2 E \rangle}{\langle m^2 \rangle} + \frac{\langle m^4 E \rangle}{\langle m^4 \rangle} \right\} \quad (13)$$

we calculate  $\left. \frac{dU_L}{dK} \right|_{K=K_c}$  at the estimated  $K_c = 0.9360$ . In Fig 4, we plot  $\frac{dU_L}{dK}$  as a function of  $L$ . From the slope of the solid line in this logarithmic plot we find

$$\frac{1}{\nu} = 1.337(16), \quad (14)$$

$$\nu = 0.7479(90). \quad (15)$$

by a least-square fit. We repeat the analysis by varying  $K_c$  within our estimated error,  $0.9360(1)$ , and find that the results for  $\nu$  are completely consistent with the result given here.

The scaling relation (12) requires a sufficiently large  $L$  to ignore the subleading corrections. In order to test if our values of  $L$  is large enough, we repeat the fits excluding the data for the smallest size  $L = 8$ , and for  $L = 8$  and  $L = 10$ . We obtain  $1/\nu(L = 8 \text{ excluded})=1.344(36)$  and  $1/\nu(L = 8 \text{ and } 10 \text{ excluded})=1.333(51)$ , respectively. Because these results are completely consistent with  $1/\nu$  with all data, we conclude that  $L = 8$  is sufficiently large to extract scaling properties.

### 3.4 The result for $\frac{\beta}{\nu}$

The scaling relation of the magnetization  $\langle |m| \rangle$  at  $K_c$  is given by

$$\langle |m| \rangle_{K_c} \sim L^{-\beta/\nu}. \quad (16)$$

We study the scaling of  $\langle |m| \rangle_{K_c}$  at  $K_c = 0.9360$  and obtain  $\beta/\nu = 0.5129(7)$  from the slope of the fitted line in Fig. 5. The fits excluding  $L = 8$ , and  $L = 8$  and  $10$  give the results consistent with this value ( $\beta/\nu(L = 8 \text{ excluded})=0.5130(15)$  and  $\beta/\nu(L = 8 \text{ and } 10 \text{ excluded})=0.5127(21)$ ). Not like the case of  $\nu$  in the previous



subsection, we find that the effect of the error of the  $K_c$  on the estimate of  $\beta/\nu$  is larger than the statistical error 0.0007 at  $K_c = 0.9360$ :

$$\begin{aligned}\frac{\beta}{\nu}(K_c = 0.9359) - \frac{\beta}{\nu}(K_c = 0.9360) &= 0.0009, \\ \frac{\beta}{\nu}(K_c = 0.9360) - \frac{\beta}{\nu}(K_c = 0.9361) &= 0.0011.\end{aligned}\quad (17)$$

Therefore we should use the value 0.0011 for the error of  $\beta/\nu$ :

$$\frac{\beta}{\nu} = 0.5129(11). \quad (18)$$

Combined with our estimate for  $\nu$ , we have

$$\beta = 0.3836(46). \quad (19)$$

### 3.5 The result for $\frac{\gamma}{\nu}$

For  $K \leq K_c$  the susceptibility  $\chi$  is defined by

$$\chi = VK \langle m^2 \rangle. \quad (20)$$

The scaling relation of  $\chi$  at  $K_c$  is given by

$$\langle \chi \rangle_{K_c} \sim L^{\gamma/\nu}. \quad (21)$$

With a similar method as in the previous sections, we obtain for  $K_c = 0.9360$   $\gamma/\nu = 1.9746(15)$  from the slope of the fitted line in Fig. 6. Again, the value of  $\gamma/\nu$  depends strongly on the choice of  $K_c$ .

$$\begin{aligned}&\frac{\gamma}{\nu}(K_c = 0.9360) - \frac{\gamma}{\nu}(K_c = 0.9359) \\ \cong &\frac{\gamma}{\nu}(K_c = 0.9361) - \frac{\gamma}{\nu}(K_c = 0.9360)\end{aligned}\quad (22)$$

$$= 0.0038. \quad (23)$$

Therefore we quote

$$\frac{\gamma}{\nu} = 1.9746(38). \quad (24)$$

Combined with our estimate of  $\nu$ , we get

$$\gamma = 1.477(18). \quad (25)$$

Using our independent results for  $\beta/\nu$  and  $\gamma/\nu$ , we can check the hyperscaling relation

$$\frac{\beta}{\nu} + \frac{1}{2} \frac{\gamma}{\nu} - \frac{d}{2} = 0. \quad (26)$$

We find

$$l.h.s. = 0.0002 \pm 0.003 \quad (27)$$

that is consistent with zero to  $O(10^{-3})$ .

### 3.6 Scaling of $\chi^c$ and $K_{\chi_{max}^c}$

To make a further check of our results for exponents, we study the finite size scaling property of the peak of the connected susceptibility  $\chi^c$ :

$$\chi^c = VK \left( \langle m^2 \rangle - \langle |m| \rangle^2 \right). \quad (28)$$

whose maximum value is expected to behave as

$$\chi_{max}^c \sim L^{(\gamma/\nu)_c}. \quad (29)$$

Here we add a suffix  $c$  for the exponent to make clear the way it is defined. Because the pseudocritical coupling constant  $K_{\chi_{max}^c}$  where  $\chi^c$  gets its maximum value is found to be slightly off the range of the applicability of the histogram reweighting method for the data at  $K_c$  (see the discussion in section 2), we carry out new simulations at  $K \simeq K_{\chi_{max}^c}$  listed in Table 1 determined by a preparatory simulation. With the histogram method applied to these new data we estimate accurate values for  $\chi_{max}^c$  and  $K_{\chi_{max}^c}$  (see Table 3). From a least-square fit shown in Fig. 7, we obtain

$$(\gamma/\nu)_c = 1.996(8). \quad (30)$$

This value is slightly larger than that from the scaling of  $\chi$ , 1.9746(38), given in (24). The same tendency is observed for the O(3) Heisenberg model [13, 18]. Because the quality of the fit for  $\chi$  is better than that for  $\chi_{max}^c$ , we quote (24) for the value of  $\gamma/\nu$ .

The scaling property of the pseudocritical coupling  $K_{\chi_{max}^c}$  provides us another test of our results:

$$K_{\chi_{max}^c}^{-1} \sim K_c^{-1} + aL^{-1/\nu}. \quad (31)$$

Using our estimate  $1/\nu = 1.337$ , we fit the data with two parameters,  $K_c^{-1}$  and  $a$ , to obtain

$$K_c = 0.9360(2). \quad (32)$$

This value is consistent with our  $K_c$  from the crossing points of the Binder cumulant.

### 3.7 Restriction of the transition point by Q value

The scaling relations (12), (16), and (21) require that the estimated value of  $K_c$  is close enough to the real transition point. If we fix  $K_c$  far from the real transition point in these scaling relations the data will not fit them well any more.

The quality of a least-square fit is determined by the Q value[19]:

$$Q(\chi^2, n) = \int_{\chi^2}^{\infty} dt \left(\frac{t}{2}\right)^{\frac{n}{2}-1} e^{-t/2} \quad (33)$$

where  $\chi^2$  is the weighted sum of squared deviations of data from the fit, and  $n = (\text{number of data points}) - (\text{number of fit parameters})$  is the degree of freedom for the fit. We may consider that the fitting procedure is appropriate if  $0.1 \leq Q \leq 0.9$ . If, on the other hand,  $Q < 0.1$  something is wrong: the error of data may be underestimated or the fitting function may be incorrect, and if  $Q > 0.9$  error of data may be over-estimated or we have too many fit parameters.

In the present case, if we fix  $K_c$  far from the real transition point, the quality of the scaling fits must become low so that the Q-value decreases to a value less than 0.1. In Fig 8 the Q-values of our finite-size scaling fits for  $\frac{dU_L}{dK}$ ,  $\langle |m| \rangle$  and  $\chi$  are plotted as a function of  $K_c$ . We find that Q-value for  $\frac{dU_L}{dK}$  is not so sensitive on  $K_c$ , while the Q-values for  $\langle |m| \rangle$  and  $\chi$  depend sensitively on  $K_c$ . This difference of the dependence on  $K_c$  between  $\frac{dU_L}{dK}$  and  $\langle |m| \rangle$ ,  $\chi$  is the same as that observed for the O(3) Heisenberg model [13]. From the condition that  $Q \leq 0.1$  we have

$$0.9359 \leq K_c \leq 0.9364. \quad (34)$$

This provides us another consistency check of our analyses. The value obtained from the crossing point of the Binder cumulant  $K_c = 0.9360(1)$  is well included in this region.

### 3.8 Comparison with the results of the $4 - \epsilon$ expansion

The critical exponents obtained in this work are compiled in Table 2 together with the values by the  $4 - \epsilon$  expansion method[6]. In our results, the exponents  $\gamma/\nu$ ,  $\beta/\nu$ , and  $\nu$  are determined independently and  $\alpha$  and  $\delta$  are calculated using (hyper)scaling relations with the value of other exponents. In the results of the  $4 - \epsilon$  expansion method,  $\eta$  and  $\nu$  are estimated independently and other exponents are calculated with  $\eta$  and  $\nu$ . Our results are completely consistent with those of  $4 - \epsilon$  with the errors reduced to about halves of them.

## 4 Conclusion

We simulated the three-dimensional O(4) Heisenberg model by applying the single-cluster algorithm, which reduces the dynamical exponent to about zero. The histogram reweighting method with high statistics data confirmed that the transition is second order for this model. We performed a precise estimation of the critical point to get  $K_c = 0.9360(1)$  from the crossing point of the Binder cumulant. The critical exponents were calculated using finite-size scaling at  $K_c$ . The exponents obtained, which are summarized in Table 2, are completely consistent with those of the  $4 - \epsilon$  method with the errors reduced to about halves of them.

We are grateful to Y. Iwasaki and A. Ukawa for valuable discussions and helpful suggestions. Numerical calculations were done on HITAC S820/80 at the National Laboratory for High Energy Physics (KEK). We would like to thank members of KEK for their hospitality and strong support, and members of the Theory Group of the Institute of Physics, University of Tsukuba, for innumerable discussions and encouragements. This project is in part supported by a Grant-in-Aid of Ministry of Education, Science and Culture (No.6206001 and 02402003).

## References

- [1] R. Pisarski and F. Wilczek, Phys. Rev. **D29**, 338 (1984).
- [2] F. Wilczek, Int. J. Mod. Phys. **A7**, 3911 (1992); K. Rajagopal and F. Wilczek, Nucl. Phys. **B399**, 395 (1993).
- [3] M. Fukugita, H. Mino, M. Okawa, and A. Ukawa, Phys. Rev. **D42**, 2936 (1990); A. Vaccarino, Nucl. Phys. B (Proc. Suppl. ) **20**, 263 (1991).
- [4] Y. Iwasaki, K. Kanaya, S. Sakai, and Y. Yoshié, Nucl. Phys. B (Proc. Suppl. ) **30**, 327 (1993).
- [5] F. Karsch, Phys. Rev. **D49**, 3791 (1994); F. Karsch and E. Laermann, Univ. Bielefeld preprint BI-TP 94/29.
- [6] G. Baker, D. Meiron and B. Nickel, Phys. Rev. **B17**, 1365 (1978); *Compilation of 2-pt. and 4-pt. graphs for continuous spin models* unpublished, University of Guelph report(1977).
- [7] R. H. Swendsen and J. -S. Wang, Phys. Rev. Lett. **58**, 86 (1987); J. -S. Wang and R. H. Swendsen, Physica **A167**, 565 (1990).
- [8] U. Wolff, Phys. Rev. Lett. **62**, 361 (1989).
- [9] U. Wolff, Nucl. Phys. **B322**, 759 (1989); U. Wolff, Phys. Lett. **B222**, 473 (1989); Nucl. Phys. **B334**, 581 (1990); Phys. Lett. **B248**, 335 (1990).
- [10] U. Wolff, Phys. Lett. **B228**, 379 (1989).
- [11] P. Tamayo, R. C. Brower, and W. Klein, J. Stat. Phys. **58**, 1083 (1990); M. Hausenbusch and S. Meyer, Phys. Lett. **B241**, 238 (1990); W. Janke, Phys. Lett. **A148**, 306 (1990).
- [12] I. R. McDonald and K. Singer, Discuss. Faraday Soc. **43**, 40 (1967) 40; A. M. Ferrenberg and R. H. Swendsen, Phys. Rev. Lett. **61**, 2635 (1988); Phys. Rev. Lett. **63**, 1195 (1989).

- [13] C. Holm and W. Janke, preprint FUB-HEP 19/92, HLRZ 77/92 (September 1992)(most detailed); preprint FUB-HEP 9/92,HLRZ 56/92, Berlin/Jülich (August 1992); Nucl. Phys. **B** (Proc. Suppl. )**30**, 846 (1993).
- [14] P. Peczak and D. P. Landau, J. Appl. Phys. **67**, 5427 (1990).
- [15] J. -S. Wang, Physica **A164**, 240 (1990).
- [16] H. G. Evertz, Nucl. Phys. **B** (Proc. Suppl.) **26**, 620 (1992).
- [17] K. Binder, Z. Phys. **B43**, 119 (1981).
- [18] P. Peczak,A. L. Ferrenberg and D. P. Landau, Phys. Rev. **B43**, 6087 (1991).
- [19] W. H. Press, B. P. Flannery, S. A. Teukolsky, and W. T. Vetterling, it Numerical recipes - the art of scientific computing (Cambridge Univ. Press, Cambridge, 1986).

$L$	simulation point ( $K$ )	sweeps/ $10^3$	$\langle C \rangle$	$\tau_m$	$\tau_c$	sweeps/ $(\tau_c \times 10^3)$
8	0.892	3000	31.6	1.95	31.6	95
8	0.935	3000	51.1	2.49	24.9	120
10	0.935	4400	78.7	2.55	32.4	136
12	0.910	4000	67.3	1.98	49.8	80
12	0.935	6000	113.2	2.48	37.7	159
14	0.912	1400	88.0	1.82	56.6	25
14	0.935	6000	154.5	2.47	43.9	136
16	0.920	3000	129.5	1.98	62.2	23
16	0.935	5200	197.4	2.32	48.1	108
24	0.926	1500	280.9	1.87	92.0	16
24	0.935	2400	427.1	2.21	71.4	34
32	0.928	1500	449.5	1.62	117.9	13
32	0.935	5600	719.1	1.95	88.9	63

Table 1: Simulation parameters and statistics.  $\langle C \rangle$  is the mean cluster volume;  $\tau_c$  is the autocorrelation time in units of sweeps, i.e. in units of the number of cluster updates;  $\tau_m$  is the autocorrelation time converted into Metropolis units, i.e. in units of updates of whole spins on the lattice:  $\tau_m = \tau_c \langle C \rangle / V$ , where  $V = L^3$  is the lattice volume.

	$4 - \epsilon$	This study
$\gamma/\nu = 2 - \eta$	1.97(1)	1.9746(38)
$\beta/\nu$	0.515(5)	0.5129(11)
$\nu$	0.73(2)	0.7479(90)
$\gamma$	1.44(4)	1.477(18)
$\beta$	0.38(1)	0.3836(46)
$\delta$	4.82(5)	4.851(22)
$\alpha = 2 - d\nu$	-0.19(6)	-0.244(27)

Table 2: Critical exponents of the three-dimensional  $O(4)$  Heisenberg model obtained by a study with the  $4 - \epsilon$  expansion method and by this study. The calculation with the  $4 - \epsilon$  expansion method is done to seven loops [6] and the results are quoted in Ref. [2]. In the  $4 - \epsilon$  method, independent calculations are done for  $\nu$  and  $\eta$ . In this study,  $\gamma/\nu$ ,  $\beta/\nu$  and  $\nu$  are determined independently. Other exponents are calculated using (hyper)scaling relations.



$L$	$K_{simu}$	$K_{\chi_{max}^c}$	$\chi_{max}^c$
8	0.892	0.8907(37)	2.118(09)
12	0.910	0.9109(05)	4.793(28)
14	0.912	0.9144(06)	6.577(48)
16	0.920	0.9183(08)	8.390(46)
24	0.926	0.9253(06)	18.89(16)
32	0.928	0.9289(01)	33.97(32)

Table 3: Results for the pseudocritical coupling  $K_{\chi_{max}^c}$  and the maximum values  $\chi_{max}^c$  of the connected susceptibility  $\chi^c$ . The  $K$  dependence of  $\chi^c$  is determined by the histogram reweighting method using the data simulated at  $K_{simu}$  on an  $L^3$  lattice.

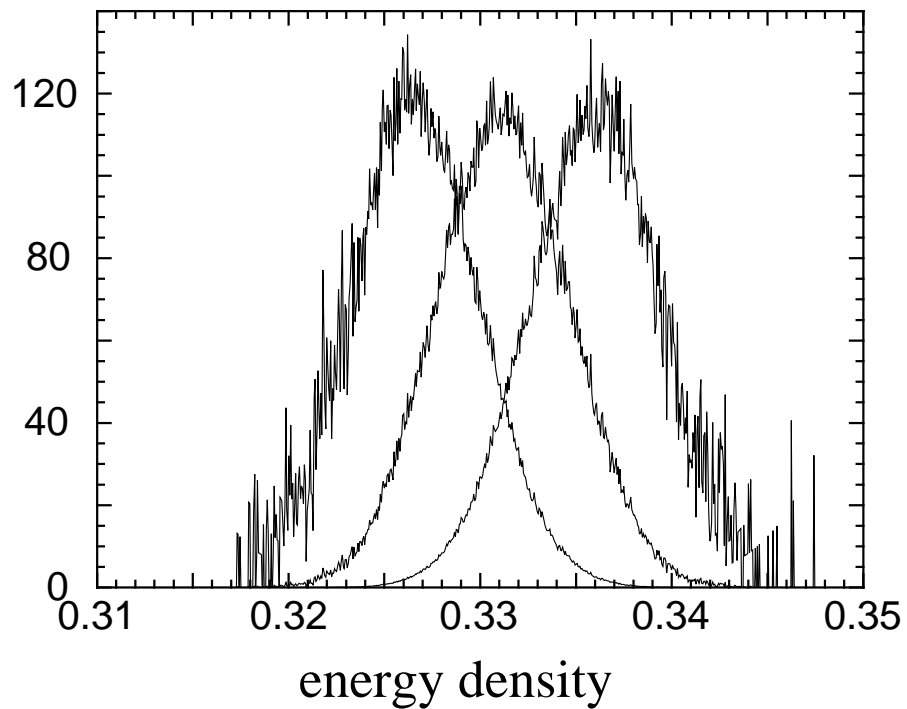


Figure 1: Histogram of the energy density for  $L=32$  near the critical coupling. Each distribution is normalized to unit area. Histograms are for  $K = 0.929, 0.935,$  and  $0.939$  from the left to the right, respectively. The histograms for  $K = 0.929$  and  $0.939$  are obtained by reweighting the measured histogram at  $K=0.935$ .

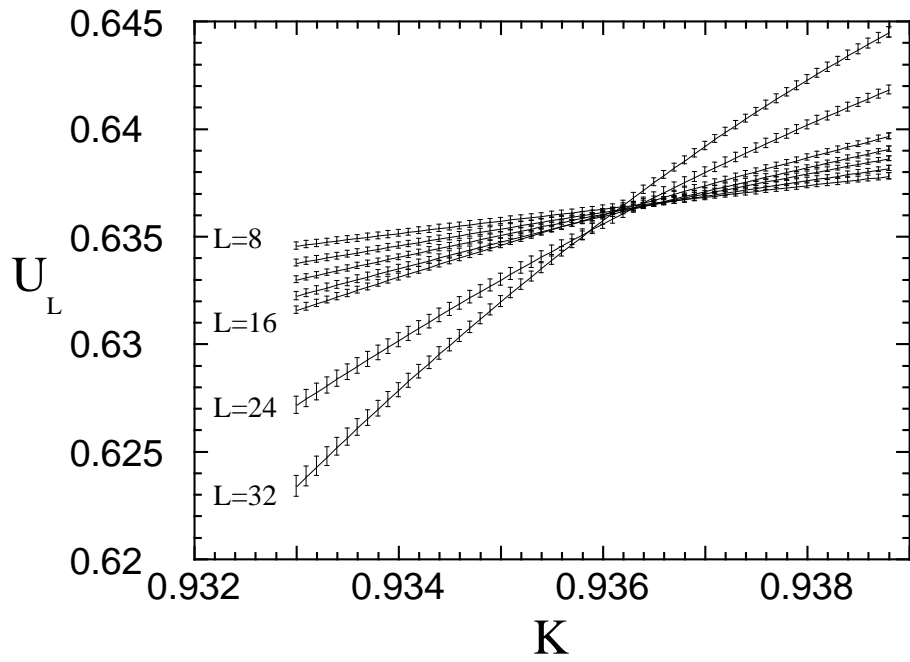


Figure 2: The Binder cumulant  $U_L$  as a function of the inverse temperature  $K$  for  $L = 8, 10, 12, 14, 16, 24$ , and  $32$ .  $U_L(K)$  is computed with the histogram reweighting method using the data at  $K = 0.935$ .

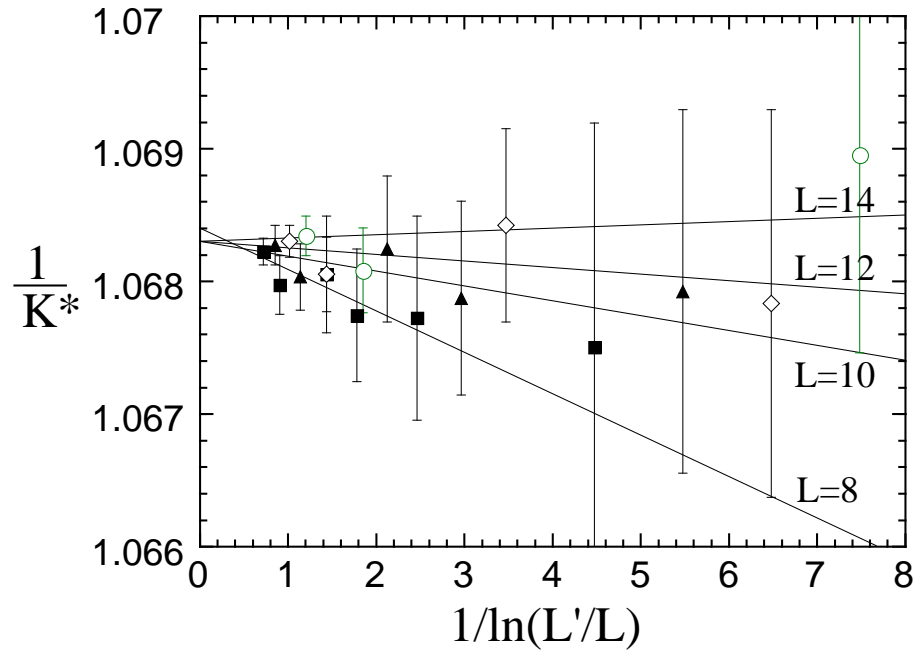


Figure 3: The crossing point of Binder cumulants  $U_L(K)$  and  $U_{L'}(K)$  for  $L = 8$ (squares),  $10$ (triangles),  $12$ (diamonds), and  $14$ (circles) with different  $L'$ . Solid lines correspond to linear least-square fits for each  $L$ . The critical coupling is estimated as  $K_c = 0.9360(1)$  by extrapolating these lines to the limit  $1/\ln(L'/L) = 0$ .

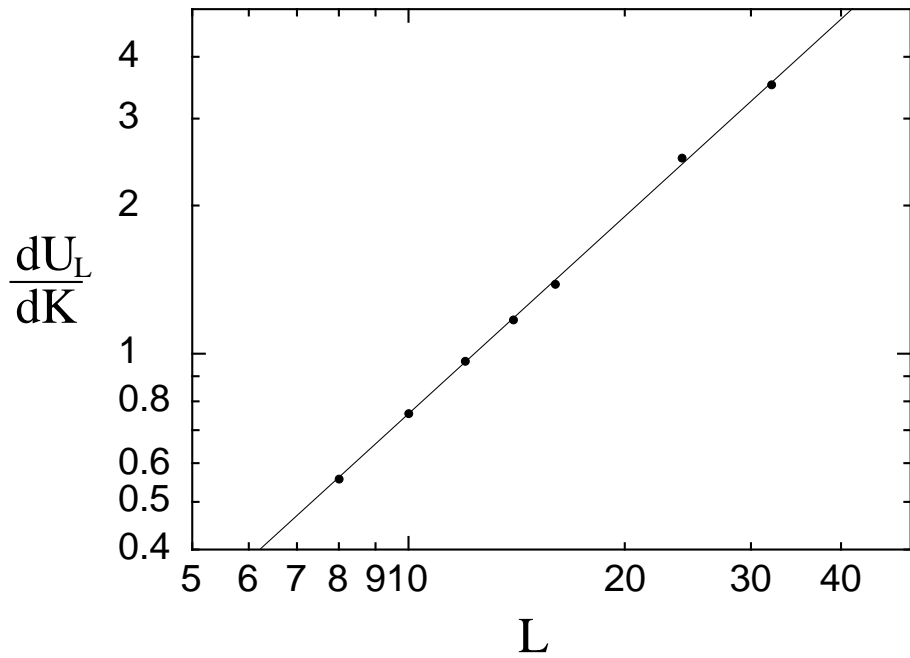


Figure 4: Scaling of the slope  $dU_L/dK$  of the Binder cumulant at  $K_c = 0.9360(1)$  as a function of the lattice size  $L$ . The slope of the solid line given by a linear least-square fit leads to an estimate of the critical exponent  $1/\nu = 1.337(16)$ . The jackknife errors for  $dU_L/dK$  are smaller than the size of symbols.

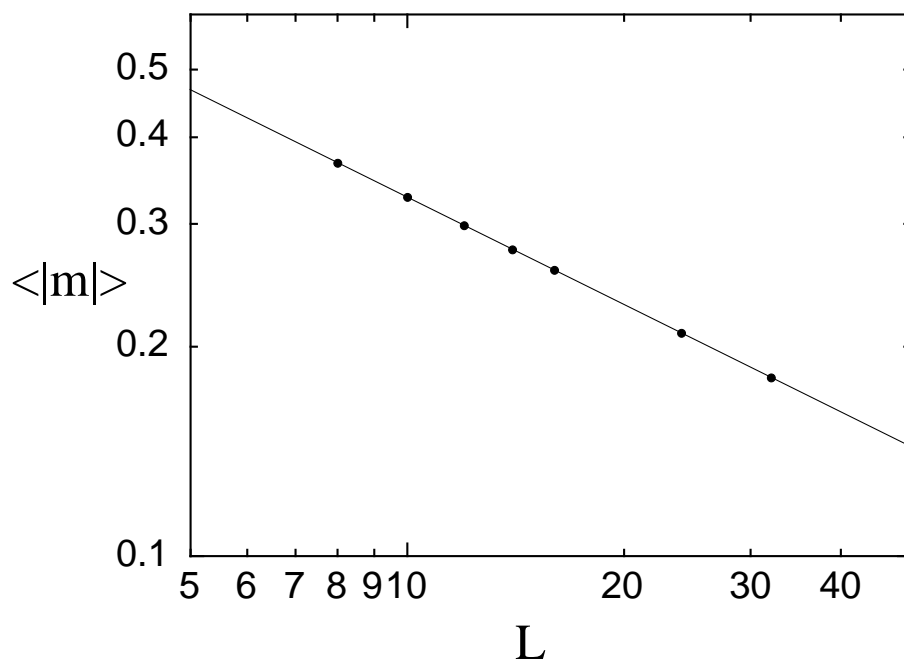


Figure 5: Magnetization  $\langle |m| \rangle$  at  $K_c = 0.9360(1)$  as a function of the lattice size  $L$ . A least-square fit gives  $\beta/\nu = 0.5129(7)$ . The jackknife errors for  $\langle |m| \rangle$  are smaller than  $1/10$  of the size of symbols.

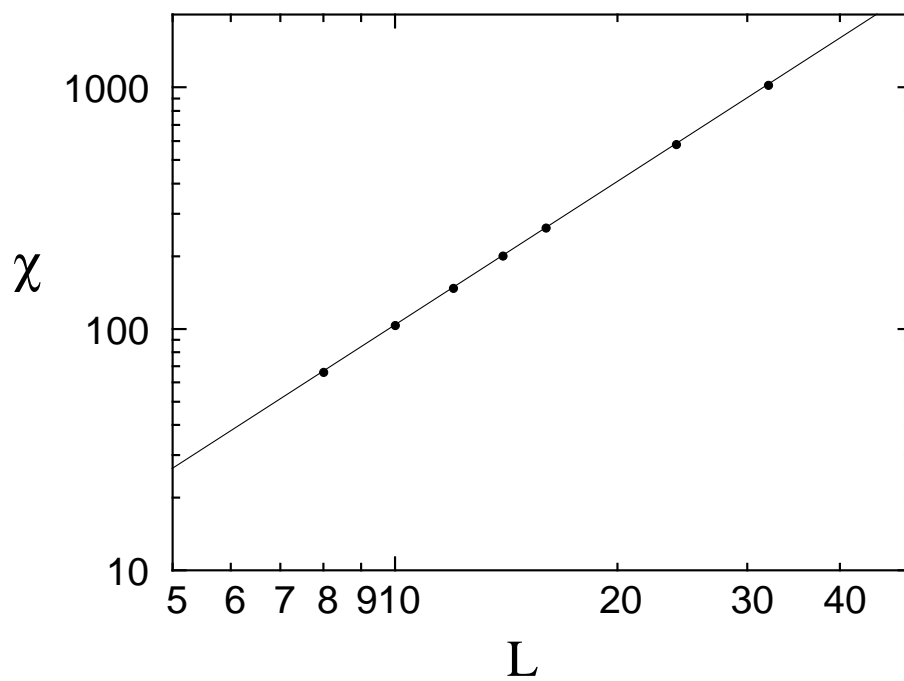


Figure 6: Susceptibility  $\chi$  at  $K_c = 0.9360(1)$  as a function of  $L$ . A least-square fit gives  $\gamma/\nu = 1.9746(15)$ . The jackknife errors for  $\chi(K_c)$  are smaller than 1/10 of the size of symbols.

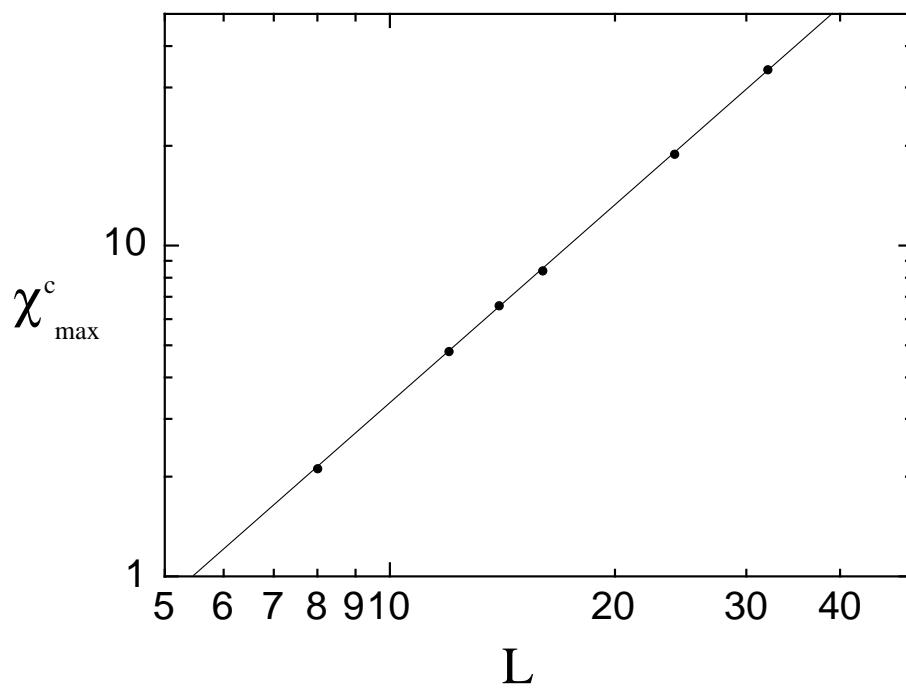


Figure 7: The maximum height of the connected susceptibility  $\chi_{\max}^c$ . A least-square fit gives  $(\gamma/\nu)_c = 1.996(8)$ . The jackknife errors for  $\chi_{\max}^c$  are smaller than 1/5 of the size of symbols.



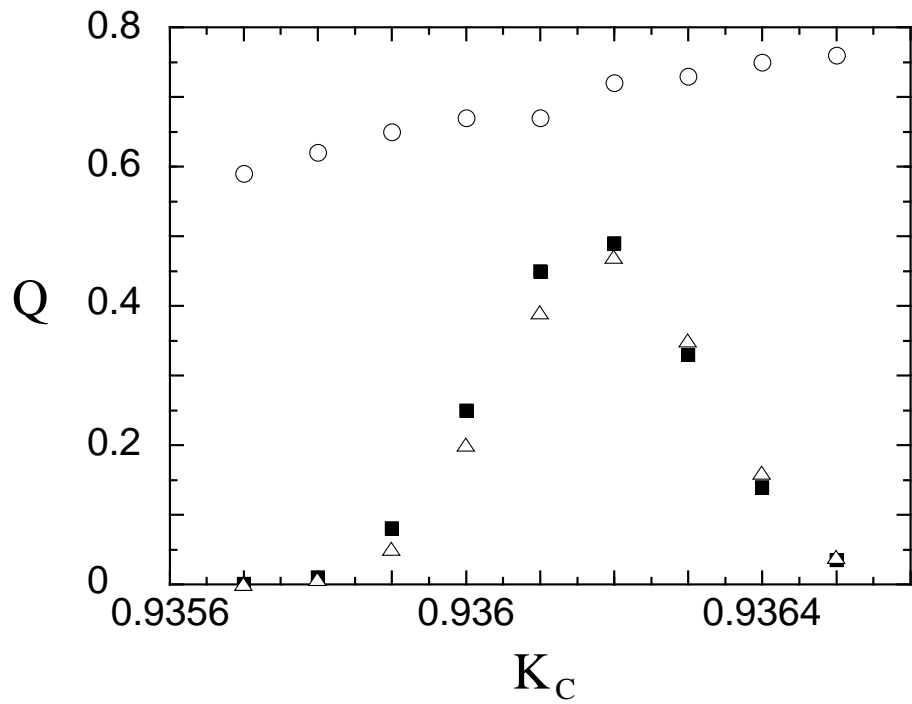


Figure 8:  $Q$  values of least-square fits for  $dU_L/dK$  (circles),  $\langle |m| \rangle$  (squares), and  $\chi$  (triangles) for various fixed  $K_c$ .